The Mu3e Experiment at PSI

Alessandro Bravar[1]⋆ on behalf of the Mu3e Collaboration

1 Département de physique nucláire et corpusculaire,
Université de Genève, Quai Ernest-Ansermet 24, Genève

⋆ alessandro.bravar@unige.ch

Abstract

Mu3e will search for charged Lepton Flavor Violation in the neutrinoless muon decay $\mu^+ \to e^+e^-e^+$ with a sensitivity down to 10^{-16} (90% C.L.) using the world most intense continuous muon beam at PSI. This search requires a large acceptance detector capable of coping with rates of up to 2×10^9 stopped muons per second with excellent momentum, spatial, and time resolution. The Mu3e detector is based on thin monolithic active silicon pixel sensors for tracking in conjunction with scintillating fibers and tiles for timing measurements. The Mu3e apparatus is under constructions and first data is expected in 2020.

1 Introduction

In the Standard Model of particle physics lepton flavor is strictly conserved. The discovery of neutrino oscillations, however, has shown that lepton flavor conservation is not a symmetry of Nature, although the observation of flavor violation in the charged lepton sector is still missing. Processes like the $\mu^+ \to e^+e^-e^+$ or the $\mu^+ \to e^+\gamma$ decays, or the $\mu^\pm A \to e^\pm A$ conversion have not yet been observed. In extensions of the Standard Model (SM) with neutrino mixing, lepton flavor violating muon decays can be mediated, for example, by loop diagrams (see Figure 1 left). Loop diagrams involving massive neutrinos, however, are strongly suppressed with branching ratios $\mathcal{O} \sim 10^{-54}$ and thus give potentially high sensitivity to charged Lepton Flavor Violation (cLFV) processes, because of the absence of SM backgrounds. Hence, any observation of cLFV would be a clear sign for new physics beyond the SM at scales far beyond the reach of direct observation, up to several PeV, as illustrated in Figure 2.

Lepton flavor conservation is naturally violated in many extensions of the Standard Model [1]. In several models [2,3] sizable cLFV effects, accessible to the new generation of high sensitivity experiments, are predicted. Several models, such as grand unified theories (GUTs), supersymmetric models (Figure 1 center), compositness, leptoquarks, left-right symmetric models, seesaw models, etc. predict an experimentally accessible amount of cLFV. cLFV can also
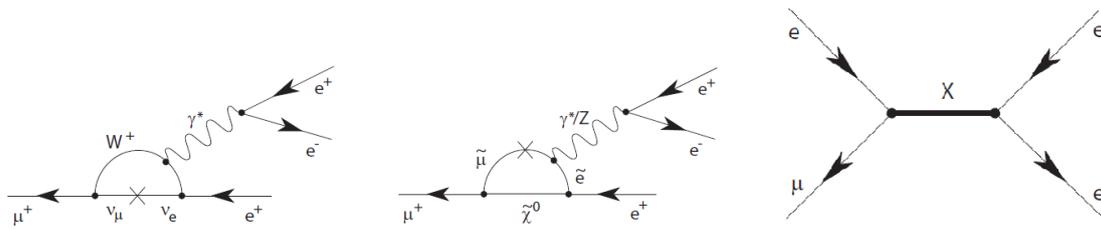
Figure 1: (left to right) Standard Model Feynman diagram for the neutrinoless $\mu^+ \to e^+ e^+ e^-$ process via neutrino mixing, diagram for cLFV involving supersymmetric particles (dipole type interaction), diagram for cLFV at tree level involving new particles (contact type interaction).

be mediated by tree couplings involving new particles (Figure 1 right) like new Higgs bosons, R-parity violating scalar neutrinos, or new heavy vector bosons, etc.

Since the discovery of the muon and the realization that the muon is the electron's *big brother*, the origin of flavor stems as one of the outstanding puzzles in elementary particle physics. Figure 3 summarizes the searches for cLFV performed by various experiments starting back in the 50's. Since none of the experiments has observed any of these processes, new upper bounds on cLFV processes have been set. Figure 3 also includes sensitivity projections for the next generation of cLFV experiments, which are about to start taking data.
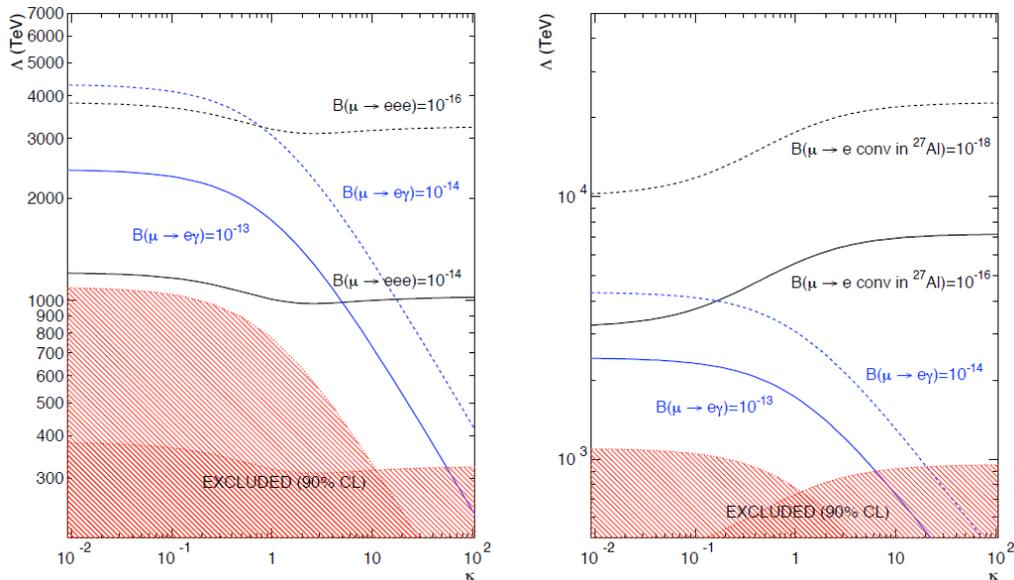
Figure 2: Reach for new physics in terms of an effective mass scale Λ in $\mu \to e\gamma$ and $\mu \to eee$ decays (left) and $\mu \to e$ conversions (right) [1] for different experimental sensitivities. κ is a parameter that weights the relative strength of dipole type contributions to four-fermion contact interactions and strictly speaking only $\kappa = 0$ (dipole int.) and $\kappa \to \infty$ (contact int.) are of interest, since it is very unlikely that different mechanisms will contribute at similar scales. The reach of the $\mu \to eee$ decay (left) for dipole type interactions ($\kappa \to 0$) could be significantly increased, if the process is mediated by the exchange of a Z boson instead of a photon.
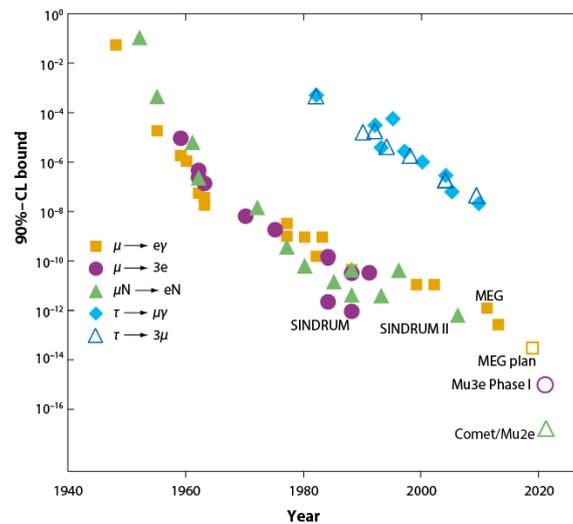
Figure 3: History of cLFV searches: evolution of upper bounds (90% C.L.) for cLFV processes set by various experiments over more than 60 years. The figure includes also sensitivity projections for the next generation of cLFV experiments, which are about to start taking data (Figure adapted from [3]).

2 The Mu3e Experiment

A new experiment to search for the cLFV neutrinoless muon $\mu^+ \rightarrow e^+e^+e^-$ decay is in preparation at the Paul Scherrer Institute [4] using the world's most intense continuous muon beamline. With a projected sensitivity of 10^{-16} (90% C.L. in the absence of a signal), Mu3e has the potential of probing new physics at the PeV scale (see Figure 2). This represents a four orders of magnitude improvement w.r.t. previous searches performed at PSI by the SINDRUM experiment [5] ($BR \leq 2.4 \times 10^{-12}$ at 90% C.L.). The cLFV decay $\mu^+ \rightarrow e^+e^-e^+$ is complementary to the $\mu^+ \rightarrow e^+\gamma$ decay and $\mu^-A \rightarrow e^-A$ conversion, since it probes different mechanisms for cLFV. It is also complementary to direct searches of Beyond the SM physics at the LHC.

Reaching this sensitivity requires:
(i) a detector with a large geometrical acceptance,
(ii) the ability to measure around 10^{17} μ^+ decays over the lifetime of the experiment,
(iii) the ability to suppress any possible background (from physics, accidentals, and reinteractions) to a level below 10^{-16}, and
(iv) a very high intensity continuous muon beam of $10^8 - 10^9$ stopped muons per second.

Experimentally the $\mu^+ \rightarrow e^+e^+e^-$ decay is identified by measuring two positrons and one electron originating from a common vertex in space and same time. In the Mu3e experiment the μ^+'s are stopped and decay at rest. Therefore, the energies of the electron and positrons sum up to the muon mass, whereas the sum of their momenta vanishes. Any other process that mimics this signature is a potential source of background and must be suppressed below the sensitivity level.

The first phase (phase I) of the experiment has been already approved and the construction of the detector has recently started after an intense R&D program. In phase I the sensitivity goal is set at $BR(\mu^+ \rightarrow e^+e^+e^-) \leq 2 \times 10^{-15}$. This sensitivity can be achieved with a muon beam intensity of 10^8 μ^+ per second, which can be provided already now by the existing PSI muon beamline. Reaching the sensitivity goal of $BR(\mu^+ \rightarrow e^+e^+e^-) \leq 10^{-16}$ will require a muon stopping rate of 2×10^9 μ^+ per second or higher.
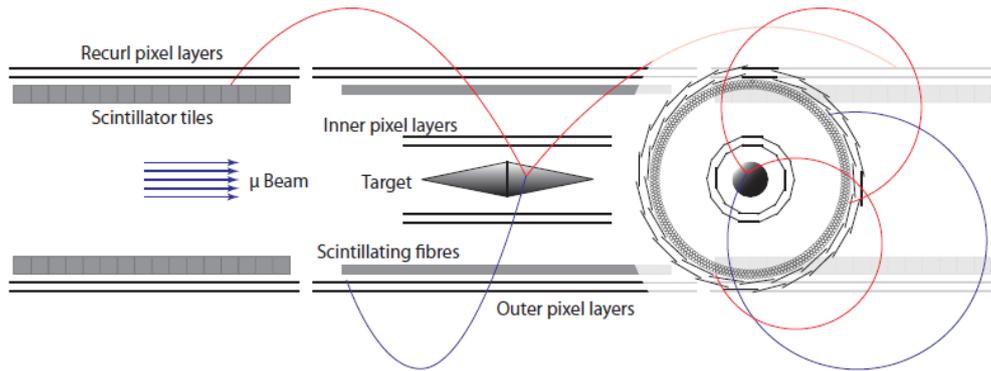
Figure 4: Schematic view of the Mu3e detector in phase I configuration (side view and cross section) showing all detector's components: the target, the inner silicon pixels, the scintillating fiber tracker, and the outer silicon pixels in the central region, and the scintillating tiles and the silicon pixels in the recurl stations. Two additional recurl stations will be added in phase II. The total length of the full detector is around 180 cm and the diameter is about 15 cm. The detector is inserted into a 100 cm diameter and 300 cm long superconducting solenoid providing a uniform magnetic field of 1 T.

2.1 The Muon Beam

The Paul Scherrer Institute (PSI) hosts the world's most intense proton beam of 590 MeV/c. The continuous surface muon beam is produced by extracting muons from the decay of pions, that were produced by impinging the proton beam on a carbon target and that decayed close to the target surface. Mu3e will be located at the πE5 beamline, which extracts and transport surface muons of 28 MeV/c. The same beamline is also used by the MEGII experiment. The compact muon beam line (CMBL), that is already installed in the experimental area of Mu3e, allows to easily switch between one experiment and the other (they will be operated alternately). It has already been demonstrated that the CMBL can provide rates of $10^8 \mu$/s. A new high intensity muon beamline HiMB is currently under investigation at PSI, with the aim to provide even higher muon beam rates. This would enable Mu3e to reach the final sensitivity goal in phase II.

2.2 Detector Design

The Mu3e detector geometry is optimized to reach the highest possible momentum resolution in a multiple Coulomb scattering environment, which is needed to suppress the dominating background from the $\mu^+ \rightarrow e^+ e^+ e^- \bar{\nu}_\mu \nu_e$ radiative decays. Minimizing the material within the acceptance of the detector is crucial to achieve these goals. Another source of background arises from the accidental combination of any two positrons and an electron that within the detector resolution shows the characteristics of the decay signal. As an example, this could be a positron from the dominant muon Michel decay $\mu^+ \rightarrow e^+ \bar{\nu}_\mu \nu_e$ in combination with a positron and electron from a Bhabha scattering event or photon conversion. The rate of the accidental background grows quadraticallly with beam intensity and can be suppressed by precise time and vertex resolution in addition to momentum resolution.

The momentum is measured via the bending radius of the particles in a magnetic field. Hence, the momentum resolution improves with the lever arm between two position measurements. The optimum momentum resolution is achieved after about a half turn, because at this point uncertainties caused by multiple scattering cancel to first order. For this reason, the Mu3e experiment relies on measuring recurling tracks. When a particle has passed the outer

detector layer, it will not cross further material and following a helical trajectory it will eventually hit the outer layers again. Between those two measurements, it has performed about a half turn.

The key elements of the Mu3e detector are illustrated in Figure 4:
(i) a high precision tracker based on HV-MAPS [6, 7], providing high spatial resolution, and (ii) a time-of-flight (ToF) system, consisting of scintillating fibers in the central region coupled to silicon photomultipliers arrays [8, 9] and scintillating tiles also coupled to Si-PMs in the outer regions, providing very precise timing information at very high particle rates.

By combining both detector technologies all backgrounds can be reduced below the aimed sensitivity of $BR(\mu^+ \rightarrow e^+e^+e^-) \sim 10^{-15}$ (see Figure 11). All elements are placed in a 300 cm long homogeneous solenoidal magnetic field of 1 Tesla. Surface muons of 28 MeV/c produced by the PSI beamline are stopped on a hollow double cone aluminum target. The design of the target maximizes the surface where muons stop and decay in order to maximize the separation of the decay verteces.

The Mu3e tracking detector is designed such to be sensitive for a transverse momentum range from 10 to 53 MeV/c (Figure 5 (left) shows the fractional coverage of the $\mu \rightarrow eee$ decay as a function of the lowest detectable positron energy) and to provide a momentum resolution better than 0.5 MeV/c over the same range, in order to suppress the $\mu^+ \rightarrow e^+e^+e^- \bar{\nu}_\mu \nu_e$ radiative decays, as shown in Figure 5 (right). This kinematical coverage corresponds to an acceptances of 50% or more for all considered cLFV models.

3   The Pixel Tracking Detector

Electrons from muon decays are detected by two cylindrical double layer silicon pixel detectors, one double layer just above the target, which allows for a precise determination of the decay vertex, and the second at a 7.5 cm radius, enabling the momentum measurement. Curling tracks are measured by a second cylindrical double layer silicon pixel detector, also at the same 7.5 cm radius, upstream and downstream of the central detector, for a total of at least 6 measured space points per track. By also measuring the curling part of the track one achieves a large lever arm.

The technology adopted for the Mu3e pixel detectors is based on the high-voltage mono-
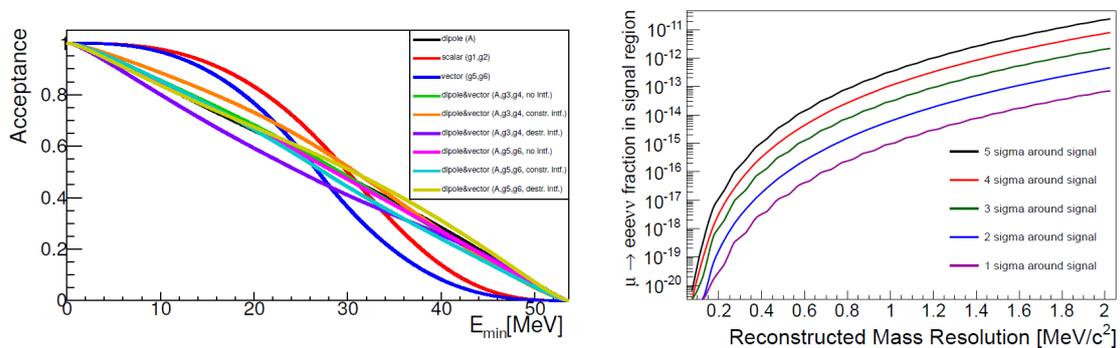
Figure 5: Coverage of the $\mu \rightarrow eee$ decay as a function of the lowest detectable positron energy for different effective cLFV models. The black line corresponds to pure dipole and the red and blue lines to pure four-fermion contact interaction models whereas the other lines correspond to a mixture of dipole and vector interactions (left). Contamination of the signal region (one sided cut) with internal conversion events ($\mu \rightarrow eee\nu\bar{\nu}$) as a function of the visible three-particle mass resolution (right).
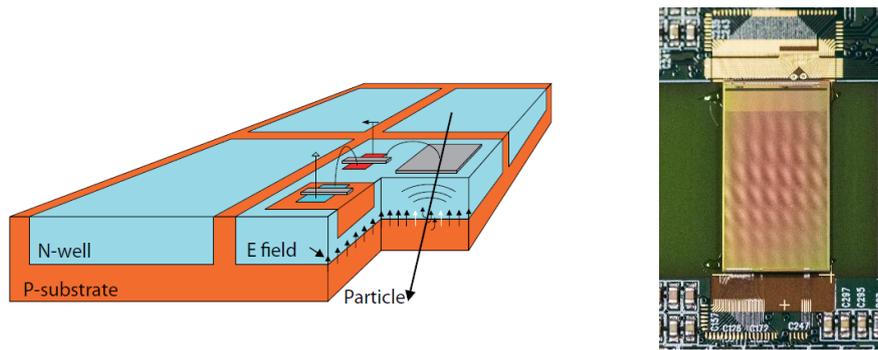
Figure 6: Schematic of a pixel sensor in HV-MAPS technology [6,7] (left) and photo of the MuPix8 sensor prototype with an active area of 19×10 mm^2 (right).

lithic active pixel sensors (HV-MAPS) in CMOS technology [6,7] (see Figure 6). The individual pixels are implemented as deep N-wells in a p-doped substrate and are reversely biased to around 80 V. Ionization charges generated by traversing particles are quickly collected within $\mathcal{O} \sim 1$ ns. The charge collection is limited to a thin depleted zone of 10 to 20 μm close to the sensor surface. Therefore, the sensors can be thinned down to 50 μm providing a very lightweight detector. Moreover it is possible to implement transistors within the pixel and thus build analog and digital logic directly on the HV-MAPS sensor itself allowing for amplification and digitization of the signals already on the chip with no additional electronics. Signal amplification and shaping is performed in the pixel itself, whereas the digitization takes place in the periphery, a small part at the bottom edge of the sensor. The sensor has digital, zero-suppressed data output with a fast serial link of 1.25 Gbit/s. A pixel size of 80×80 μm^2 is planned for the final sensor with an active area of 2×2 cm^2 per sensor. The development of the sensors is in the final prototyping stage. With a pixel size of 80×80 μm^2 the HV-MAPS tracker will consists of 180 million pixels (phase I).

Figure 7 illustrates the performance of the MuPix8 sensor prototype with an active area of 2×1 cm^2 and a pixel size of 80×81 μm^2 (very close to the final design). This prototype has been thinned down to 60 μm. The sensor has been extensively tested, yielding efficiencies in excess of 99% with very low noise, little cross-talk, and few dead pixels. In order to improve the timing resolution, the MuPix8 incorporates also signal amplitude measurements allowing to correct for time-walk. A time resolution of around 14 ns has been achieved after time-walk corrections.
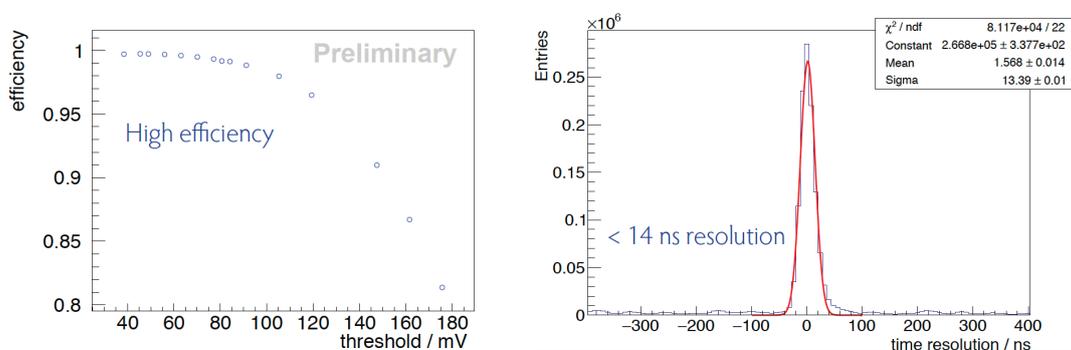
Figure 7: Performance of the MuPix8 pixel sensor prototype: efficiency (left) and time resolution (right) obtained in testbeam measurements.
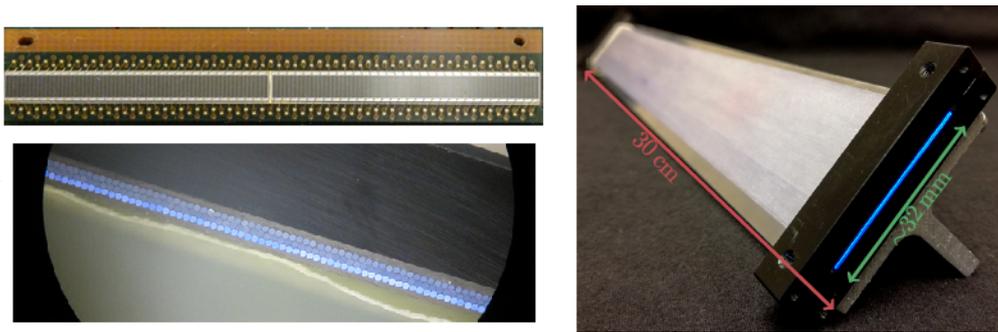
Figure 8: 128 ch. Si-PM array used for the readout of scintillating fibers (top left), microscope photo of a three layer staggered SciFi ribbon profile (bottom left), and SciFi ribbon prototype close to the final size (right).

4 The Timing Detectors

The combinatorial backgrounds can be efficiently suppressed by timing measurements. For this purpose, the silicon tracker is complemented by a cylindrical time of flight (ToF) detector consisting of a very thin scintillating fiber tracker in the central region and scintillating tiles in the recurl stations. The scintillating fiber detector (SciFi) is placed directly below the outer pixel layers. The main role of the ToF system is to measure very precisely the time of production of various particles in order to reject pile-up events (accidental backgrounds) with very high efficiency. With the combination of timing information from the fiber and tile detectors, background suppression factors of about 100 with two correlated and one uncorrelated track can be achieved. Backgrounds with three uncorrelated tracks are even more strongly suppressed. In addition, the SciFi detector will help to determine the charge of the recurling tracks in the central region of the apparatus by determining the sense of rotation for charged tracks.

Figure 8 shows the components of the SciFi detector. The SciFi arrays are formed by staggering 3 layers of double clad 250 μm diameter scintillating fibers (Figure 8 bottom left), for an overall thickness smaller than 0.2% of a radiation length. The SciFi tracker consists of 12 ribbons (Figure 8 right), 30 cm long and 32 mm wide. The ribbons are arranged cylindrically at a 6 cm radius. The fibers are read out at both end with 128 channel Si-PM arrays (Figure 8 top left). By arranging the individual cells of the Si-PM into columns one obtains a sensor consisting of 250 μm wide independent readout channels with a common cathode.

Different scintillating materials have also been evaluated, as shown in Figure 9 left. In
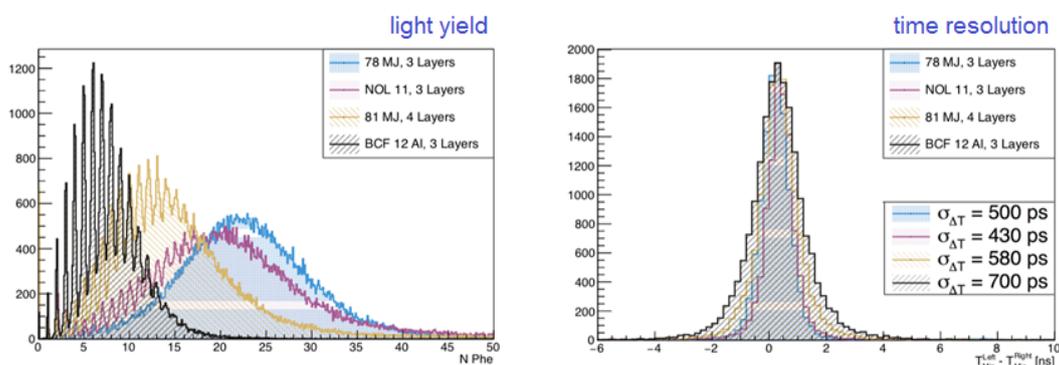
Figure 9: Characterization of different scintillating fibers: light yield (left) and measured time resolution (right).
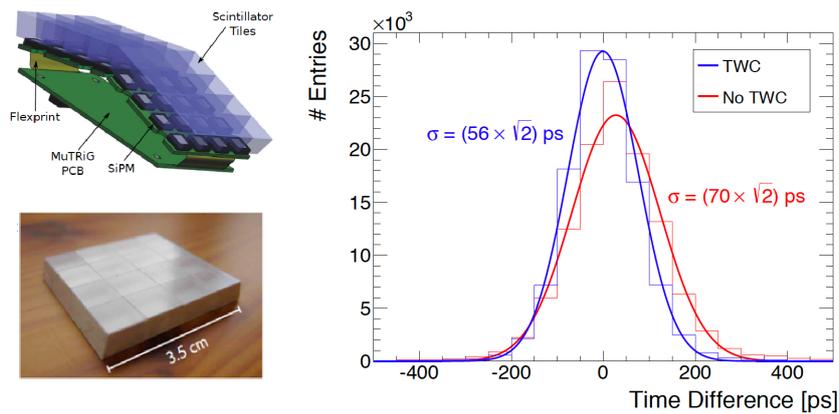
Figure 10: Overview of the scintillating tile detector in the recurling stations of the Mu3e apparatus: design of the detector (top left), the scintillating tile matrix (bottom left), and achieved time resolution (right).

testbeam studies an efficiency in excess of 96% with a spatial resolution of around 80 μm have been achieved for the three layer SciFi detector. Figure 9 (right) shows the time difference measured from both fiber ends for crossing particles. The crossing time is obtained by taking the meantime of both time measurements resulting in a time resolution two times better than for the time difference (i.e. half of the value reported in Figure 9). The best timing so far achieved is of 200 ps.

The curling tracks are measured a second time in the recurl stations. Figure 10 left illustrates the design of the scintillating tile detector, which consists of $8 \times 8 \times 8$ mm^3 scintillating cubes coupled individually to 3×3 mm^2 Si-PMs. Figure 10 right shows the time resolution obtained for this detector. With time walk corrections a resolution better than 60 ps can been achieved. The SciFi arrays and the tiles are read out with a dedicated mixed mode ASIC, the MuTRiG, capable of sustaining rates in excess of a MHz per readout channel.

5 Mu3e Sensitivity

The final sensitivity of the Mu3e experiment depends on the ability to reduce accidental backgrounds, and irreducible backgrounds (physics) such as the $\mu^+ \to e^+ e^+ e^- \bar{\nu}_\mu \nu_e$ radiative decays. In addition, one has to also identify and reject reinteractions in the detector materials. Accidental backgrounds can be efficiently suppressed by excellent timing (few 100 ps) and vertex resolution. The suppression of physics backgrounds requires high momentum resolution ($\sigma_E < 0.5$ MeV) in order to reconstruct precisely the μ^+ decay kinematics. The following criteria will be exploited:

(i) energy and momentum conservation (all 3 outgoing electrons are coplanar with zero total momentum and the total energy reproduces the parent muon mass),

(ii) vertex reconstruction (all 3 tracks originate from the same point), and

(iii) timing (all 3 tracks are produced in a very narrow time window).

Figure 11 illustrates the ability of the proposed Mu3e detector to separate the $\mu^+ \to e^+ e^+ e^-$ signal at different branching ratios from the radiative decay with internal conversion and accidental combinations of electrons from Bhabha scattering and Michel decays. The detector performs well enough to separate signal $\mu^+ \to e^+ e^+ e^-$ decays from background even at a branching ratio of 10^{-15}.
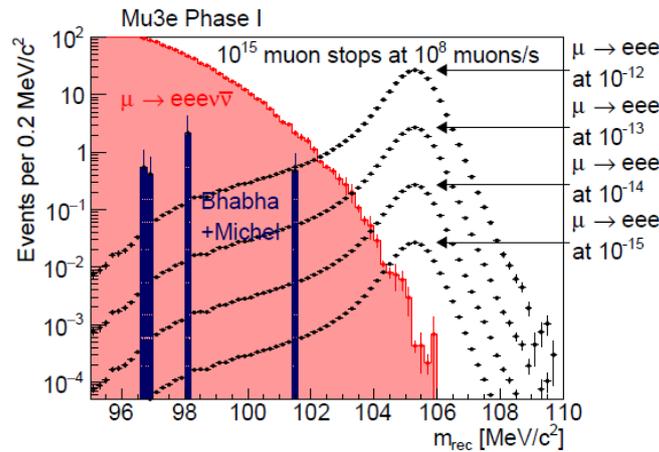
Figure 11: Reconstructed mass of three electrons from simulated internal conversion events, accidental combinations of Bhabha scattering events and Michel decays. In comparison, the $\mu \to eee$ decay signal at various branching ratios is also shown.

6 Summary

Many different prototypes of the various sub-detectors have been successfully tested and the results obtained have proven the suitability of the chosen technologies for the Mu3e experiment. The Mu3e collaboration is finalizing the detector design and preparing for construction and commissioning of the experiment. Commissioning is expected in 2019 with potential first physics data taking in 2020.

In the first phase of Mu3e, a single event sensitivity of 10^{-15} is expected. This represents already a significant improvement (3 orders of magnitude) w.r.t. existing limits on the LFV $\mu^+ \to e^+e^+e^-$ decay [5] and in absence of a LFV signal will set new stringent limits on new physics models. The final envisaged sensitivity of Mu3e of 10^{-16} will be reached in a second phase, which will require an upgrade of the phase I detector and a new muon beamline providing muon stopping rates in excess of $2 \times 10^9/\text{s}$.

References

[1] A. de Gouvêa and P. Vogel, *Lepton flavor and number conservation, and physics beyond the standard model*, Prog. Part. Nucl. Phys. **71**, 75 (2013), doi:10.1016/j.ppnp.2013.03.006.

[2] Y. Kuno and Y. Okada, *Muon decay and physics beyond the standard model*, Rev. Mod. Phys. **73**, 151 (2001), doi:10.1103/RevModPhys.73.151.

[3] W. J. Marciano, T. Mori and J. Michael Roney, *Charged lepton flavor violation experiments*, Annu. Rev. Nucl. Part. Sci. **58**, 315 (2008), doi:10.1146/annurev.nucl.58.110707.171126.

[4] A. Blondel et al., *Research proposal for an experiment to search for the decay $\mu \to eee$* (2013), arXiv:1301.6113.

[5] U. Bellgardt et al., *Search for the decay $\mu^+ \to e^+e^+e^-$*, Nucl. Phys. B **299**, 1 (1988), doi:10.1016/0550-3213(88)90462-2.

[6] I. Perić, *A novel monolithic pixelated particle detector implemented in high-voltage CMOS technology*, Nuclear Instrum. Methods Phys. Res. Sect. A **582**, 876 (2007), doi:10.1016/j.nima.2007.07.115.

[7] I. Perić, C. Kreidl and P. Fischer, *Particle pixel detectors in high-voltage CMOS technology—New achievements*, Nucl. Instrum. Methods Phys. Res. A **650**, 158, doi:10.1016/j.nima.2010.11.090.

[8] B. Beischer et al., *A high-resolution scintillating fiber tracker with silicon photomultiplier array readout*, Nucl. Instrum. Meth. A **622**, 542 (2010), doi:10.1016/j.nima.2010.07.059.

[9] A. Damyanova and A. Bravar, *Scintillating fiber detectors for precise time and position measurements read out with Si-PMs*, Nucl. Instrum. Meth. A **845**, 475 (2017), doi:10.1016/j.nima.2016.06.088.